

HYDROGASIFICATION OF HYDRANE CHAR IN FLUIDIZED AND MOVING BEDS

C. Y. Wen,* S. Mori,* J. A. Gray,** and P. M. Yavorsky**

*West Virginia University
Morgantown, West Virginia

**U.S. Bureau of Mines
Pittsburgh Energy Research Center
Pittsburgh, Pa. 15213

ABSTRACT

To satisfy future pipeline gas requirements, considerable process development work is being aimed at gasifying coal to produce substitute natural gas (SNG). The heart of many of the gasification processes being developed is a fluid-bed gasifier in which char is reacted with steam/oxygen or hydrogen. In the HYDRANE process, being developed at the U.S. Bureau of Mines, Pittsburgh Energy Research Center, char is reacted directly with hydrogen in the fluid-bed stage of the hydrogasifier. In order to scale-up the fluid-bed reactor to pilot plant or commercial size with confidence, a fluid-bed reactor model has been developed using the bubble-assemblage concept and has been shown to fit existing data reasonably well. Data from moving-bed reactor experiments and the corresponding model were compared to the fluid-bed results and illustrate the differences between plug-flow and well-mixed solid-gas reactors.

INTRODUCTION

In order to satisfy future pipeline gas requirements and alleviate current shortages, considerable process development work is underway for gasifying coal to produce substitute natural gas (SNG). The heart of many of the gasification processes under development is a fluid-bed gasifier in which char is reacted with steam/oxygen or hydrogen. In the HYDRANE process (figure 1), being developed at the U.S. Bureau of Mines, Pittsburgh Energy Research Center, raw coal of bituminous or lower rank is reacted directly with hydrogen in a two-stage hydrogasifier to produce 95% of the product methane. The lower stage of the hydrogasifier is a fluidized bed of char in which hydrogen is the fluidizing gas. Conceptually,

the gas exiting the bed contains about 46% methane, and the char leaving the fluid bed contains about half the carbon initially fed to the hydrogasifier in the raw coal. Prevention of agglomeration is of great importance because most of the eastern and midwestern American coals soften, swell, and become sticky at temperatures above 400° C., especially in the presence of hydrogen, and are therefore impossible to process in a fluid bed without some pretreatment or dilution. Thus, the top stage of the hydrogasifier is a dilute-phase, free-fall reactor in which the raw pulverized coal is fed in a dilute cloud concurrently with the gas produced in the bottom stage, rendering the particles nonagglomerating and producing a very porous, reactive char. Approximately 20% to 30% carbon conversion occurs in this stage, and the product gas contains about 70% methane.

Experimental data have been obtained from a 12 lb./hr. process development unit in which the bottom stage of the hydrogasifier has been operated as either a fluidized bed or a moving bed reactor. In designing a scaled-up version of the fluid-bed reactor, a model describing the movement of gas and solids in the reactor and a reaction rate model is needed. The reactor model is then integrated with the reaction rate equation yielding reactor size and product gas composition. In this paper a fluid-bed reactor model has been developed using the bubble-assemblage concept originally developed by Kato and Wen (1) and is shown to describe some experimental data reasonably well. A moving-bed reactor model is also developed and used to model experimental data as well as illustrate the differences between plug-flow and well mixed solid-gas reactors.

Apparatus and Procedure

The two-stage laboratory hydrogasifier is shown in figure 2. It consists of a dilute-phase reactor integrated with a second stage which can be operated as either a moving-bed or fluid-bed reactor. The dilute-phase reactor is a 3-inch-diameter, schedule 10, type 304, stainless steel pipe 6-feet long. The pipe is heated in three 2-feet-long sections containing six 1,000-watt strip heaters

mounted directly on the pipe wall. The pipe is wrapped in fiberfrax insulation and is contained in a 10-inch-diameter, schedule 160, carbon steel pipe which acts as the pressure shell. Pulverized coal is fed into the reactor by gravity via a 1/4-inch nozzle which protrudes one foot into the reactor. When the second stage was operated as a fluid bed, the char leaving the dilute-phase reactor was crushed to reduce the particle size to a level acceptable for fluidization. The average diameter of char particles leaving the dilute-phase reactor can be as much as six times the average diameter of the pulverized feed coal particles owing to swelling and particle agglomeration and consequently, prevent adequate fluidization unless the particles are crushed. An example of particle swelling is shown in table 1. The second stage reactor is also a 3-inch-diameter pipe, but is 10-feet long and has five heated zones. A sleeve having a 2-inch inside diameter is inserted into the 3-inch-diameter pipe for fluidized-bed experiments. Temperatures reported for the dilute-phase and fluid-bed reactors correspond to reactor pipe wall thermocouple measurements. In the moving-bed experiments, reported temperatures correspond to thermocouples suspended directly into the char bed.

Two fluid-bed reactor schemes were used and are shown in figure 3. In scheme A, hydrogen was fed without preheating into the bottom of the bed by two gas nozzles, and residual char was removed at the bottom of the bed. A small amount of fines was carried over in the interstage gas. The bed level was measured by three pressure differential probes which were continually purged with a nitrogen flow of about 6 s.c.f.h. Some typical temperature profiles are shown in figure 4 and indicate that about 30 cm. of the fluid bed is required to heat up the hydrogen feed gas and attain a uniform bed temperature. In scheme B, the hydrogen was preheated to reactor temperature and was fed through a distributor plate at the bottom of the reactor. The preheater temperature and hence hydrogen feed temperature was controlled closely by a cooling water coil inside the preheater itself and extending the full length of the preheat zone.

TABLE 1.- Typical Particle Data for Dilute-Phase Char
(Illinois #6 h.v.C.b.) Before Crushing*

Run No.	162	163	164
<u>U.S. Mesh Size</u>	<u>Wt. %</u>	<u>Wt. %</u>	<u>Wt. %</u>
On 1/4"	0.05	0.03	0.05
1/4" x 4	1.16	0.57	0.49
4 x 6	8.96	4.89	5.62
6 x 8	17.35	14.77	10.27
8 x 10	12.09	12.09	10.81
10 x 12	8.47	8.91	8.51
12 x 14	8.34	8.89	9.40
14 x 20	17.35	19.34	20.00
20 x 30	13.27	13.78	17.76
30 x 50	9.52	10.52	14.31
50 x 100	3.11	5.47	2.45
100 x 200	0.18	0.47	0.18
Thru 200	0.15	0.25	0.18
\bar{d}_p , mm.	1.031	0.866	0.897
ρ_b , gm./cm. ³	0.109	0.141	0.111

*Feed Coal 50- x 100-mesh (U.S. Sieve Size), \bar{d}_p = 0.223 mm.

The residual char was carried out of the reactor with the product gas via an overflow pipe and was separated from the gas. A baffle was inserted at the top of the reactor to prevent short-circuiting of feed char directly to the overflow pipe. Typical temperature profiles for this mode of operation are illustrated in figure 5. Again about 30 cm. of bed was needed to achieve a uniform temperature because too much cooling water was circulated through the preheater.

The reactor scheme for the moving-bed experiments is shown in figure 6. The char from the dilute-phase reactor dropped into the second-stage reactor which consisted of a free-fall zone and a moving-bed zone. Hydrogen was fed into the bottom of the moving-bed zone and flowed countercurrent to the movement of char. Char was removed from the bottom of the reactor by a starwheel crusher and the residence time was varied by changing the char bed height. Typical temperature profiles for this scheme are shown in figure 7.

In all experiments except HY-3, the carbon conversion was determined from an ultimate analysis of the char product and the composition of the initial coal assuming 100% ash recovery. In some experiments, the recovery of carbon, ash, and hydrogen were checked and were usually better than 95%. The moving-bed product gas composition was not known accurately because product gas from the dilute-phase reactor, containing about 70% methane, mixed with the moving-bed product gas near the sampling point. This yielded inflated values of methane concentration. Therefore, methane yields based on the moving-bed product gas analysis were not used. The mixing effect is shown in figure 8 where actual and calculated methane concentrations are shown. Carbon conversion for the overall two-stage unit based on the solids analysis was checked by calculating carbon conversion based on the total product gas and oil yields.

The ultimate analyses for the Illinois #6 h.v.C.b. coal and the char product for the fluid-bed tests and the char particle data are tabulated in table 2. The

TABLE 2.—Ultimate Analysis (as-received) of Illinois #6 h.v.C.b. Coal and Charcoal Particle Data for Fluid-Bed Tests

Run No.	2	3	4	5	6	7	8	9	10	11	12	13	14
	Wt. %												
	Coal	Char	Coal										
C	70.8	75.1	71.8	67.7	70.9	66.0	63.8	53.7	62.4	50.8	64.7	61.6	63.8
H	5.1	2.0	5.1	2.1	4.8	1.6	4.3	0.7	4.3	0.9	4.4	0.8	4.3
N	1.7	0.8	1.6	1.1	1.7	0.9	1.4	0.5	1.4	0.4	1.4	0.4	1.4
S	1.4	0.4	1.2	0.7	0.7	0.7	1.4	0.6	1.3	0.6	1.3	0.6	1.4
O	12.8	2.3	11.7	9.7	10.0	7.0	8.9	1.1	9.4	1.8	12.0	1.9	10.4
Ash	8.2	19.4	8.6	18.7	11.3	23.8	20.2	43.4	21.2	41.5	16.2	34.7	18.7
VH	34.7	6.1	34.4	6.6	34.4	3.8	30.8	3.1	30.4	1.1	30.5	2.8	36.8
Moisture	3.0	6.0	2.5	5.7	1.0	5.3	1.1	0.4	0.7	0.4	1.4	2.3	1.7
U.S. Mesh Size													
6 x 12													
12 x 20	0.5		0.7		0.2		8.3		2.7		10.0		4.7
20 x 30		2.2		3.4		2.8		26.8		20.9		31.4	
30 x 50		18.8		26.5		23.7		19.3		18.6		16.3	
50 x 80		22.7		27.4		27.1		22.6		29.8		22.7	
80 x 100		6.7		8.5		8.2		13.1		17.8		16.2	
100 x 140		4.8		5.5		4.0		4.0		4.3		2.4	
140 x 200		5.0		3.1		2.3		3.3		3.5		2.0	
$\frac{d}{d^2}$, mm.													
200	35.4		25.6		30.3		1.0		1.6		1.6		0.9
P _b , gm./cm. ³	0.109		0.135		0.124		0.406		0.442		0.356		0.401
	0.179		0.179		0.179		0.131		0.123		0.112		0.188

corresponding run conditions and conversion data are listed in table 3. The carbon conversion in the dilute-phase reactor for tests HY-2, 3, 13, and 14 was assumed to be about 28% based on previous dilute-phase data with Illinois #6 coal (2), and the remaining conversion occurred in the fluid bed. For tests HY-5, 11, and 12, essentially pure hydrogen was used as the feed gas instead of a hydrogen-methane mixture so that an additional 4.5 to 5% carbon conversion occurred bringing the dilute-phase value to 33%. The conversion of the other coal constituents in the dilute-phase reactor can be calculated using the correlations given in figures 9-12, which are based on 95 coal hydrogasification experiments in the HYDRANE PDU. The data for sulfur removal are scattered because of the error in determining changes in small amounts of sulfur in the coal and char samples. Oxygen removal, which usually exceeds 90% for carbon conversions above 20%, can be considered to be complete. The calculated constituent conversions in the dilute-phase reactor for 28% and 33% carbon conversion are shown in table 4.

The ultimate analyses for the Illinois #6 h.v.C.b. coal used in the moving-bed tests and the analyses of the char product are shown in table 5. These data are presented on a dry basis for convenience in calculating conversions.

Reaction Rate of Coal-Char Hydrogasification

It has been demonstrated by a number of investigators (3,4,5,6,7,8) that coal consists roughly of two portions greatly differing in reactivity: a highly reactive portion relating to the volatile hydrocarbons present in coal, and a relatively low reactivity residual carbonaceous matter, coke. In the presence of hydrogen, the initial phase of extremely rapid reaction is presumably due to pyrolysis followed by hydrogenolysis of the intermediates that are derived from essentially aliphatic hydrocarbon side chains and oxygenated functional groups. The remainder of the carbon in the char is converted to methane much more slowly, apparently at the char surface almost stoichiometrically according to the graphite-hydrogen reaction.

TABLE 3.- Solids Conversion For Fluid-Bed Tests, 50- x 100-Mesh
Illinois #6 h.v.C.b. Coal, 1,000 p.s.i.g.

Run	2	3	5	11	12	13	14
Coal Rate, gms./hr. (Dry)	2270	2724	4631	5448	3087	2951	3042
<u>Dilute-Phase Reactor</u>							
Temp., ° C	850	850	850	850	900	900	900
Feed Gas, s.c.f.h.	234	185	260	167	108	110	110
% H ₂	45	56	94.5	93	92.6	53.4	47.8
CH ₄	48	35	0.2	0	0	38.0	39.0
Ar(He*)	6	8	4.3	7	7.4	7.3*	11.0*
N ₂	1	1	1.0	0	0	1.2	1.2
<u>Fluid-Bed Reactor</u>							
Feed Gas, s.c.f.h.	310	215	320	330	249	240	240
% H ₂	97	94	99	91	91.1	88	88
N ₂	3	6	1	9	8.6	12	12
<u>Total Conversion</u>							
C	55.2	53.6**	55.8	60.8	55.1	55.6	53.7
H	88.2	79.9	89.8	92.7	89.6	94.0	90.1
S	87.9	71.8	74.4	80.1	76.4	78.4	82.3
N	80.1	66.3	74.9	83.4	85.4	86.7	82.3
O	97.2	77.8	88.1	95.6	91.6	100	100
Fluid-Bed Height, cm.	143	143	143	122	122	122	122
Char Yield, gm./gm. dry coal	0.436	0.499	0.480	0.471	0.514	0.473	0.503

**Calculated based on char recovered.

TABLE 4.- Calculated Constituent Conversion in
the Dilute-Phase Reactor

Conversion, %		
C	28.0	33.0
H	65.2	69.6
S	47.5	51.2
N	29.6	38.7
O	92.5*	93.0*
Char Yield, gm./gm. dry coal	0.677	0.639

*Estimated from Figure 13.

TABLE 5.- Ultimate Analysis (Dry Basis) of Illinois #6 Coal in Moving-Bed Tests

Run No.	Ultimate Analysis (Dry Basis) of Illinois #6 Coal in Moving-Bed Tests					Ultimate Analysis (Dry Basis) of Illinois #6 Char From Moving-Bed Tests				
	33	37	38	39	43b	44b	45b	46a	48	49
	Wt. %	Wt. %	Wt. %	Wt. %	Wt. %	Wt. %	Wt. %	Wt. %	Wt. %	Wt. %
C	70.41	68.70	66.67	67.97	66.25	67.67	67.57	66.77	66.01	67.43
H	4.57	4.59	4.56	4.51	4.41	4.48	4.53	4.45	4.42	4.44
N	1.73	1.32	1.43	1.44	1.44	1.45	1.46	1.45	1.46	1.46
S	1.53	2.34	1.53	1.75	1.65	2.17	1.88	1.97	1.98	2.08
O	11.04	10.65	10.47	10.11	10.50	7.09	9.45	9.67	9.77	9.72
Ash	10.71	12.40	15.34	14.21	15.74	17.15	16.16	15.68	16.16	14.67
VH	34.7	35.5	34.0	34.7	34.3	35.1	34.5	34.4	35.0	32.8
Moisture	2.0	1.6	2.2	2.9	2.8	3.2	4.1	3.7	4.1	3.9
=										
Run No.	33	37	38	39	43b	44b	45b	46a	48	49
	Wt. %	Wt. %	Wt. %	Wt. %	Wt. %	Wt. %	Wt. %	Wt. %	Wt. %	Wt. %
C	67.91	75.40	67.30	70.49	67.44	67.52	59.59	68.61	65.65	64.63
H	1.18	0.96	1.04	1.53	1.29	1.30	1.73	1.80	0.32	0.60
N	1.01	0.70	0.60	1.01	0.91	0.82	1.12	1.23	0.30	0.41
S	0.71	0.50	0.60	1.01	1.21	0.92	1.42	1.33	1.01	1.02
O	1.95	0.04	0.37	0.68	1.03	1.77	1.02	0.25	0.00	2.05
Ash	27.23	22.39	30.08	25.28	28.11	27.78	35.13	26.79	32.72	30.28
VH	3.8	1.8	2.7	3.9	3.7	4.1	7.0	6.9	1.3	1.7
Moisture	1.2	0.4	0.6	0.7	1.1	2.1	1.5	2.2	0.7	1.9

During the initial phase of the coal-hydrogen reaction, the coal particles are quickly softened, become metaplastic giving off volatile matter, and erupt in a manner somewhat similar to popping of popcorn. Wen and Huebler (7) presented a kinetic model for this initial rapid reaction of coal hydrogasification. In the free-fall reactor of the HYDRANE process, the initial phase of hydrogasification of coal takes place leaving a small portion of volatile matter in the char. This char is then reacted with hydrogen in a fluidized-bed reactor in the HYDRANE process. The reaction rate in this second phase of hydrogasification has been described elsewhere (7,9,10).

For the second phase reaction,



where λ is a stoichiometric coefficient obtained by an empirical correlation (9,11)

$$\lambda = \begin{cases} 1.0 & \text{for } X < 0.45 \\ 8X - 2.6 & \text{for } 0.45 \leq X \leq 0.55 \\ 1.8 & \text{for } 0.55 < X \end{cases} \quad (2)$$

and the average value of λ is obtained as follows:

$$\bar{\lambda} = \int \lambda \, dX / \int dX \quad (3)$$

The rate of hydrogasification of char is given by

$$\frac{dZ}{dt} = k(1-Z)P_{\text{H}_2} \quad (4)$$

where Z is the carbon conversion in the second phase reaction and is equal to $(X - X_0)/(1-X_0)$. Here X is the carbon conversion based on the raw coal, X_0 is the carbon converted in the first phase reaction or in the pretreatment, P_{H_2} is the partial pressure of hydrogen and k is the reaction rate constant.

The above equation can be written in the following form as

$$\frac{dZ}{dt} = K(1-Z) Y_{\text{H}} \quad (5)$$

where $Y_{\text{H}} = P_{\text{H}_2}/P_{\text{H}_2}^{\circ}$, $K = kp_{\text{H}_2}^{\circ}$ and $P_{\text{H}_2}^{\circ}$ is the partial pressure of hydrogen at the inlet.

Feldmann et al (12) presented the following correlation for the reaction rate constant:

$$\ln k = -10.45 \times 10^3 \left(\frac{1}{T} \right) + 7.08, \quad k: \text{ atm.}^{-1} \text{hr.}^{-1}, \quad T: \text{ K}$$

As will be shown later, the values of k and activation energy calculated from experimental carbon conversions using the Bubble Assemblage model or moving bed model developed are significantly smaller than those calculated from the above equation.

Simulation of Fluidized-Bed Hydrogasifier

1. Minimum Fluidization Velocity

It has been shown by Feldmann et al (12,13) that the minimum fluidization velocity of coal chars with popcorn-like structure is greater than that calculated from the Wen-Yu correlation (14) which is applicable only to nonvesicular particles. The empirical correlation proposed by Feldmann et al (13) has the following form:

$$\frac{u_{mf}}{\mu} = 0.0135 \left[d_p^3 \frac{\rho_f(\rho_s - \rho_f)}{\mu^2} g \right]^{0.73} \quad (6)$$

where d_p is particle diameter,

ρ_f is gas density,

ρ_s is particle density,

μ is gas viscosity

g is gravitational acceleration, and

u_{mf} is the minimum fluidization velocity.

2. Fluidized-Bed Model

In the fluidized bed hydrogasifier, the second-phase reaction takes place either countercurrently, concurrently, or with overflow as schematically described in figure 13. The Bubble Assemblage model (1,15,16,17,18) is used to simulate the hydrogasification of coal char. The essential features of the Bubble Assemblage model are summarized as follows:

- The fluidized bed is divided into a number of compartments, each of which has a height that is uniquely determined by the diameter of the bubble at the corresponding height.
- Each compartment is composed of the bubble phase and the emulsion phase. The solids and gas in the emulsion phase and the bubble phase of each compartment are completely mixed with some exchange of gas between the two phases.
- The volume of the bubble phase is assumed to be equal to the volume of the bubbles in this paper. It is also assumed that no solids exist in the bubble phase.

Figure 14 depicts the Bubble Assemblage Model under various modes of flow arrangement. P_c is an index of solid flow arrangement and is equal to unity when solids flow countercurrent to the gas. Under this condition, $q_1 = 1 + q_2$, where q_1 and q_2 are the ratio of solids downflow rate and solids upflow rate to the solid feed rate, respectively.

When solids are fed from the top and withdrawn from the top of the bed (overflow type), P_c is 0 and $q_1 = q_2$.

From the material balance of H_2 around the n -th compartment in the bed, the following equations can be written for the bubble phase and emulsion phase.

$$W_{HO} (Y_{Bn-1} - Y_{Bn}) + V_{Bn} Y_{HO} F_{On} (Y_{en} - Y_{Bn}) = 0 \quad (7)$$

$$V_{Bn} Y_{HO} F_{On} (Y_{Bn} - Y_{en}) - V_{en} k_b Y_{en} (1 - Z_n) = 0 \quad (8)$$

where k_b is an apparent reaction rate constant for H_2 consumption in the emulsion phase and can be written as

$$k_b = \alpha_c (1 - \epsilon_{mf}) \rho_{CO} Y_{CO} K \quad (9)$$

α_c is the number of moles of H_2 reacted with one gram of carbon in char and is related to $\bar{\lambda}$ as $\alpha_c = \bar{\lambda}/12$.

From a material balance of carbon in the char around the n -th compartment, excluding $n=1$ and N , the following equation can be obtained,

$$q_1 W_{SO} Y_{CO} (Z_{n+1} - Z_n) + q_2 W_{SO} Y_{CO} (Z_{n-1} - Z_n) = -V_{en} k_b Y_{en} (1-Z_n)/\alpha_c \quad (10)$$

For the top compartment of the bed ($n=N$), we get $Z_{N+1} = 0.0$ and the following equation is obtained:

$$-q_1 W_{SO} Y_{CO} Z_N + W_{SO} Y_{CO} \left[q_2 Z_{N-1} - (1-p_c) Z_N \right] = -V_{en} k_b Y_{en} (1-Z_N)/\alpha_c \quad (11)$$

For the first compartment ($n=1$), the following equation can be written for the overflow type and the countercurrent type:

$$W_{SO} Y_{CO} (q_1 Z_2 - p_c Z_1) - q_2 W_{SO} Y_{CO} Z_1 = -V_{en} k_b Y_{en} (1-Z_1)/\alpha_c \quad (12)$$

From equations (7) and (8) we obtain:

$$Y_{Bn} = Y_{Bn-1} \left[1 - \frac{\alpha_2 (1-Z_n)}{1 + (1+\alpha_1) \alpha_2 (1-Z_n)} \right] \quad (13)$$

$$Y_{en} = -(Y_{Bn} - Y_{Bn-1})/\alpha_2 (1-Z_n) \quad (14)$$

where $\alpha_1 \equiv F_t/V_{Bn} F_{on}$ and $\alpha_2 \equiv V_{en} k_b / W_{HO}$.

From equations (10), (11), (12), and (14) we get:

$$Z_{n+1} = \left[(q_{11} + q_{21}) Z_n - q_{22} Z_{n-1} + \alpha_3 (Y_{Bn} - Y_{Bn-1})/\alpha_2 \right] / q_{12} \quad (15)$$

where $Z_o = Z_{N+1} = 0.0$, $\alpha_3 \equiv V_{en} k_b / \alpha_c W_{SO} Y_{CO}$ and the values of q_{ij} are given in table 6.

If the solid particles in the bed are assumed to be completely mixed, the basic equation can be simplified as follows:

$$Z_n = Z_{1F} = \text{constant}$$

$$Y_{BN} = \sum_{j=1}^n \left[1 - \frac{\alpha_2 (1-Z_{1F})}{1 + (1+\alpha_1) \alpha_2 (1-Z_{1F})} \right] j \quad (16)$$

where Z_{1F} is the conversion in the bed and at the outlet.

From an overall material balance, another equation relating Y_{BN} and Z_{1F} can be obtained as follows:

TABLE 6.- q_{ij} in equation (15)

	q_{11}	q_{12}	q_{21}	q_{22}
$n \neq 1, N$	q_1	q_1	q_2	q_2
$n = 1$	p_c	q_1	q_2	0.0
$n = N$	q_1	1.0	$1-p_c$	q_2

$$Z_{1F} = \alpha_3 (1 - Y_{BN}) / \alpha_2 \quad (17)$$

From Hovmand and Davidson (19), if the value of $G_f \equiv (u_o - u_{mf})/0.35 \sqrt{gD_t}$ is less than 0.2, the bed can be kept in freely bubbling condition. When the value of G_f is greater than 0.5, the bed is in a slug flow condition. When G_f is between 0.2 to 0.5, the bed is in a transition condition between bubbling flow and slug flow.

Recently, Mori and Wen (17,18) presented a new correlation of bubble growth for a bubbling bed as follows:

$$D_B = D_{BM} - (D_{BM} - D_{B0}) \exp(-0.3 h/D_t) \quad (18)$$

where D_{BM} is the maximum bubble diameter, D_{B0} is the initial bubble diameter and h is the elevation above the distributor.

Since the fluidized gasification unit used has a large bed height to diameter ratio ($L_f \gg D_t$), equation (18) can be simplified as follows:

$$D_B \sim D_{BM} = 0.652 \{A_t (u_o - u_{mf})\}^{0.4} \quad (19)$$

Then, the height of each compartment in the bed, Δh_n , also can be approximated as:

$$\Delta h_n = D_B = D_{BM} \quad (20)$$

From Kato and Wen (1), the gas interchange coefficient, F_{on} , is given by

$$F_{on} = 11/D_B \quad (21)$$

Based on the two-phase theory, volume fractions of bubble phase and emulsion phase in each compartment are given as follows, respectively:

$$\epsilon_{Bn} = V_{Bn} / \Delta h_n A_t = (u_o - u_{mf}) / u_B \quad (22)$$

$$V_{en} = (1 - \epsilon_{Bn}) \Delta h_n A_t \quad (23)$$

Since the solid particles may be assumed to be transferred upward in the wakes behind the bubbles, the volumetric flow rate of solids upward can be written as $f_W (u_o - u_{mf}) (1 - \epsilon_{mf}) A_t$, where f_W is the volume ratio of the wake and the bubble.

Thus, q_2 can be rewritten as,

$$q_2 = \frac{(u_o - u_{mf}) f_W (1 - \epsilon_{mf}) A_t}{W_{so}/\rho_{co}}$$

Using equations (19), (20), (21), (22), (23) and (24) the values of V_{Bn} , V_{en} , F_{on} , q_2 and Δh_n can be calculated for a set of operating conditions. Thus, numerical solutions of equations (13), (14), and (15) are obtained simultaneously by an iterative method. A computer logic diagram is shown in figure 15.

Results of Fluidized-Bed Performance Simulation

In table 7, the calculated reaction rate constants are shown based on the experimental carbon conversions. The values of reaction rate constants from the Bubble Assemblage Model and those from the simplified Bubble Assemblage Model with complete mixing of solids are compared. As for the axial solids mixing, the large height to diameter ratio of the experimental reactor used results in a relatively small degree of solid mixing. The following equation derived by Miyauchi (20) for a backflow mixing model is used to estimate the Peclet number for counterflow case,

$$\frac{1}{N_{Pe}} = \frac{E_{zp}}{(W_{so}/\rho_{co} A_t) L_f} = \frac{1}{2N} + \frac{q_2}{N} \quad (25)$$

where N is the total number of compartments. For the overflow case, an analogy of equation (25) is used to calculate the Peclet number:

$$\frac{1}{N_{Pe}} = \frac{q_2}{N} \quad (26)$$

In table 8, the values of $\frac{1}{N_{Pe}}$ are tabulated and vary between 0.3 to 1.2, considerably different from the large values obtained for complete mixing. As can be seen from table 7, the k values of countercurrent operation calculated from the Bubble Assemblage model with partial mixing of solids differ very little from the Bubble Assemblage model with complete mixing of solids indicating that the solid mixing does not affect carbon conversion significantly. The reaction rate constants are plotted on an Arrhenius Plot shown in figure 16 based on

TABLE 7.- Comparison of Reaction Rate Constants Calculated from Bubble Assemblage Models

Run No.	Solid Flow	X_{1F}	Z_{1F}	Bed temp. K	$k_{cal.}$, atm ⁻¹ hr ⁻¹	
		observed	observed		Solid partial mixed	Solid complete mixed
11		0.608	0.419	1073	0.0450	0.0515
12	counter current	0.551	0.335	1118	0.0202	0.0220
13		0.556	0.383	1113	0.0218	0.0248
14		0.537	0.357	1183	0.0139	0.0152
2		0.552	0.378	1158	0.0145	0.0123
3	over-flow	0.536	0.356	1158	0.0284	0.0140
5		0.558	0.345	1158	0.0316	0.0223

TABLE 8.- Estimated Solid Mixing in Fluidized-Bed Hydrogasifier in Terms of Peclet Number

Run No.	N	q_2	$1/N_{pe}$
11	32	19.9	0.64
12	34	25.1	0.76
13	39	20.3	0.53
14	41	25.8	0.64
<hr/>			
2	38	46.4	1.22
3	54	16.0	0.30
5	40	20.5	0.51

N = total number of compartments.

N_{pe} = Peclet number of axial solid mixing in the fluidized bed.

the average temperatures of the bed. The data include the results of I.G.T. experiments (7) shown in table 9 for countercurrent and concurrent fluidized-bed hydrogasification experiments. The complete mixing model is used for calculation of the reaction rate constants for the I.G.T. experiments. The reaction rate constants calculated from moving-bed data are also plotted in figure 16.

An empirical relation for the temperature effect on the rate constant can be expressed as,

$$\ln k = -4.36 \left(\frac{1}{T} \right) \times 10^3 + 0.28 \quad (27)$$

where k : atm.⁻¹ hr.⁻¹, and T : K .

An activation energy of 8.63 Kcal/mole is estimated which is very much smaller than 15-16 and 21 Kcal/mole reported by Feldmann et al (12).

The rate constants calculated from the moving-bed data are considerably larger than those from the fluidized bed, particularly in the low temperature region. An explanation of the deviation is presented in the moving-bed section. In figure 17, the carbon conversions calculated using equation (27) are compared with experimental conversions. The scatters of the points shown in figures 16 and 17 are partly due to the nonuniformity and time dependency of temperature along the bed axis.

Moving-Bed-Reactor Model

In this model the gas and solid are assumed to move in a plug flow manner and the temperature profile of the bed is averaged to approximate an isothermal reactor. The movement of char through the moving bed, $v_s = \frac{dh}{dt}$, is assumed to be constant and can be combined with equation (3) to yield an equation describing the carbon conversion in terms of position in the moving bed ($h = 0$ at top of bed),

$$v_s \frac{dz}{dh} = kp_{H_2} (1-z) \quad (28)$$

The carbon conversion in the countercurrent moving bed can be related to the change in methane content of the gas by the carbon balance equation,

TABLE 9.- Operating Condition of I.G.T. Experiments
[Wen and Huebler (1965)]

Operation	Countercurrent	Concurrent
Char.	Consolidation Coal Co. Bituminous coal char	
d_p	60/325 mesh	
D_t , cm.	4.88	4.3(equivalent)
T, K	905 - 958	992 - 1189
U_{mf} , cm./sec. . .		1.83
W_{co} , g./sec. . . .	0.61 - 1.07	0.28 - 1.05
F_t , cm ³ /sec. . . .	57 - 111	29 - 54
P_T , atm.		137 - 141
L_f , cm.	214	143, 225

$$Y_{CO} W_{SO} \frac{dz}{dh} = - \frac{d}{dh} (W_g Y_M) \quad (29)$$

where W_{SO} is the dry coal feed rate to the dilute-phase reactor (gm./hr.), X_0 fractional carbon conversion in the dilute-phase reactor, Y_{CO} the gm. moles of carbon per gram of dry coal, W_g the molar gas rate (gm.-moles/hr.), and Y_M the mole fraction of methane in the gas. We have made the assumption that the conversion of carbon to CO or CO_2 in the moving bed will be negligible. Previous work with char appears to support this assumption (6,21). The partial pressure of hydrogen is given by

$$P_{H_2} = (n - Y_M) P_T \quad (30)$$

where P_T is the total pressure and n is the combined mole fraction of hydrogen and methane in the gas. The difference of n from unity represents the mole fraction of inert in the gas. The net change in the molar gas rate is

$$\frac{dW_g}{dh} = (\lambda - 1) Y_{CO} W_{SO} \frac{dz}{dh} \quad (31)$$

Equations (29) and (31) may be integrated over an arbitrary distance h starting at the top of the moving bed resulting in the equations

$$W_{GO} Y_{MO} - W_g Y_M = Y_{CO} W_{SO} Z \quad (32)$$

$$W_g - W_{GO} = Y_{CO} W_{SO} \int_0^Z (\lambda - 1) dZ \quad (33)$$

Evaluation of equations (32) and (33) using the boundary conditions $Z = Z_H$, $Y_M = 0$ and $W_g = W_{gH}$ at $h = H$ yields values for W_{GO} and Y_{MO} . Once W_{GO} and Y_{MO} are known, Y_M and W_g can be evaluated at any point in the moving bed. Thus, the mole fraction of methane at any position h is given in terms of the carbon conversion as

$$Y_M = \frac{W_{GO} Y_{MO} - Y_{CO} W_{SO} Z}{W_{GO} + Y_{CO} W_{SO} \int_0^Z (\lambda - 1) dZ} \quad (34)$$

Henceforth the integral in the denominator will be written as $F(Z)$. Substitution of equations (30) and (34) into equation (28) and integrating over the length of the bed, H , yields the following relationship for the reaction rate constant k :

$$k = \frac{1}{P_T \theta} \cdot \int_0^H \frac{[1 - BF(Z)]}{[A + B(1-Z) - nBF(Z)][1-Z]} dZ \quad (35)$$

where $\theta = V_s / H$

$$A = n - Y_{Mo} - B$$

$$B = -\frac{Y_{co} W_{so}}{W_{go}}$$

Equation (35) can be solved analytically in one, two, or three parts, depending on the evaluation of λ in equation (1). The solution of equation (35) is shown in Appendix A.

Moving-Bed Results

The conversion of the coal constituents are plotted in figure 18 versus residence time in the moving bed. Zero residence time corresponds to solid material free-falling through the dilute-phase reactor followed by free-fall through the empty moving-bed reactor. Such a condition should approximate the conversion in the dilute-phase reactor plus that in the free-fall portion of the moving-bed reactor when a char bed level is maintained. Char conversion in the free-fall section of the moving-bed reactor is probably low because the reactivity is much lower compared to the starting coal and the residence time is less than a second. Zero residence time tests yielded a carbon conversion of 30%, and this value is used as X_0 in the moving-bed model calculations. These results are summarized in table 10 and the rate constants are shown on figure 16 as an Arrhenius plot. The effect of temperature on the moving-bed rate constant values can be described by the

TABLE 10.- Countercurrent Moving-Bed Kinetic Data, Illinois #6

Run	Total C** Conv.	Moving Bed Conv.	Dry Coal Rate, gm./hr.	Feed Gas Rate, mole hr.	Product Gas Rate, mole hr.	Total Pressure, atm.	Residence Time, min.	Rate Const., atm. ⁻¹ hr. ⁻¹	Temp., °C
33*	.620	.457	3178	133.9	116.0	69.0	20	.0573	905
37	.392	.131	6497	173.5	173.5	66.6	3.8	.0360	900
38	.485	.264	5262	163.2	161.8	68.7	7.3	.0396	875
39	.417	.167	6170	191.9	191.9	68.4	4.0	.0449	645
43b	.430	.186	4654	177.9	177.9	68.4	5.1	.0395	765
44b	.391	.130	4985	178.5	178.5	68.7	5.1	.0260	650
45b	.406	.151	4998	174.9	174.9	68.7	5.1	.0307	660
46a	.399	.151	4772	173.6	173.6	68.7	5.1	.0305	684
48	.511	.301	4540	177.0	173.3	68.7	10.5	.0299	800
49	.536	.337	4685	176.6	168.8	68.1	10.0	.0358	715

*n = 0.67; other tests, n = 1

**X_o = 0.300, Z = (X - X_o)/(1 - X_o)

equation

$$\ln k = -2.21 \left(\frac{1}{T}\right) \times 10^3 - 1.19 \quad (36)$$

The discrepancy between the moving-bed and fluid-bed data in figure 16 was first believed to be a result of hydrogen mass transfer resistance between the bulk gas and the char particle surface. The Reynolds number for the moving-bed tests ranged from 0.882 to 1.146 while the Schmidt number varied from 0.569 to 0.933. Using these values and available mass transfer correlations, the mass transfer coefficient, k_g , was estimated to be 0.119 to 0.132 moles H_2 /hr.cm.²atm. Correction of these values to the same form as k yielded mass transfer coefficients in excess of 1,400 atm.⁻¹hr.⁻¹ confirming that particle film resistance was not a significant factor. The discrepancy is believed to be a result of heat transfer resistance from the char particles to the bulk gas phase resulting in the particle temperature being higher than the temperature of the gas and the measured bed temperature. This can be verified by a simple heat transfer model if we assume the reaction rate, the average particle temperature, and the average gas temperature in the bed are constant, and the heat generated by reaction is distributed uniformly within the particles. A heat balance around a particle gives the equation

$$\frac{dT_p}{d\eta} = \frac{h_f A_p \theta}{\rho_p C_p s} (T_g - T_p) + \frac{A_T H}{C_p s} Q_T \quad (37)$$

where the equation for the heat generation rate per unit volume of bed, Q_T is

$$Q_T = \frac{(-\Delta H) Z_1 Y_{CO} W_{SO}}{A_T H} \quad (38)$$

Using the boundary conditions $T_p = T_g$ when $\eta = 0$ ($t = 0$) and $T_p = T_{p1}$ when $\eta = 1$ ($t = \theta$) the solution of equation (37) is,

$$\frac{T_{p1}}{T_g} = (1 + \frac{\beta}{\delta}) - (\frac{\beta}{\delta}) e^{-\delta} \quad (39)$$

where $\delta = \frac{6h_f(1-\varepsilon)\theta}{\rho_b T_p d_p}$

$$\beta = \left[\frac{z_1 Y_{CO} (-\Delta H)}{T_g \bar{C}_{ps}} \right] \frac{W_{SO}}{W_s}$$

Evaluation of equation (39) using the parameter values listed in table 11 yields

$T_{p1}/T_g = 1.2$ and $T_{p1} = 1120$ K. This means the temperature of the particles at $t = \theta = 30.6$ sec. is 187 K above the temperature of the gas, which is 933 K.

The log-mean average temperature of the particles is 990° K, so that on the average the difference in temperature between the gas and particles is 57 K for this case. Thus, the moving-bed k values at the lower temperatures in figure 16 should be more toward the left since the particle temperature was probably higher than the gas temperature. The measured temperature approximates the gas temperature since the gas channels along the thermocouple sheath sweeping its surface to a large extent. The contact area between the char particles and the thermocouple sheath is small compared to the area swept by the gas.

CONCLUSIONS

Hydrogasification reaction rate constant values were calculated using partial mixing and complete mixing versions of the Bubble Assemblage model of the fluidized bed. These results indicated that solid mixing did not have a significant effect on the carbon conversion. This was not unexpected because the carbon conversions in the bed were under 40%. Thus, the reactor was operating in a regime where changes in axial mixing exhibit only a minor influence on conversion. The k values for the complete mixing model with countercurrent operation are slightly higher than the values for the partial mixing model because the carbon content in the

TABLE 11.- Parameter Values Used in Equation 39

u_0	2.5 cm./sec.	C_{Pf}	3.5 cal./gm. K
T_g	933 K	Z_1	0.10
θ	30.6 sec.	Y_{co}	0.68
d_p	0.04 cm.	Pr	12.6
ρ_b	0.15 gm./cm. ³	Re	1.11
\bar{C}_{ps}	0.4 cal./gm. K	Nu	0.01
ρ_f	4×10^{-3} gm./cm. ³	h_f	2.5×10^{-5} cal./cm. ² sec. K
μ_f	3.6×10^{-4} poise	δ	1.0
k_f	1.0×10^{-4} cal./cm.sec. K	β	$0.3 \frac{W_{so}}{W_s} \sim 0.3$
$-\Delta H$	1.5 x 10^3 cal./gm. carbon reacted		

completely mixed bed is lower than in most locations in the partial mixed bed, thus, requiring a larger rate constant in order to obtain the same amount of conversion. In the case of overflow operation of the fluid bed, larger k values are obtained for the partial mixing case than for complete mixing because some of the char particles have a very short retention time in the bed before overflowing out. The k values must then be larger in order to obtain the same conversion as the complete mixing case.

Mixing was important, however, from the standpoint of heat removal from the char particles and maintaining an approximately isothermal bed. The importance of heat removal was very evident in the moving-bed results where heat transfer from the char particles was apparently poor, causing the particle temperature to be higher than the measured temperature. This effect was dominant in the low-temperature region where moving-bed k values were significantly larger than fluid-bed k values. This heat transfer problem may be the reason why Feldmann, et al (12) obtained large values of k and a large activation energy when they fit the kinetic model given by equation (3) to the moving-bed data of Lewis, et al (21). Obviously, hydrogasification data is best obtained in a fluidized bed or in a thermobalance such as that used by Johnson (22) where the reaction heat can be removed so the char temperature is equivalent to the gas temperature and is isothermal.

NOMENCLATURE

A_p	specific surface area, $A_p \approx (1-\varepsilon) \frac{6}{d_p}$, $\text{cm.}^2/\text{cm.}^3$
A_t	cross sectional area of the bed, cm.^2
\bar{C}_{pf}	average heat capacity of gas, cal/gm. K
\bar{C}_{ps}	average char heat capacity, cal/gm. K
d_p	particle diameter, cm.
E_{Zp}	axial solid dispersion coefficient, $\text{cm.}^2/\text{sec.}$

F_{on}	gas interchange coefficient per unit volume of bubble phase in n -th compartment, sec. ⁻¹
F_t	volumetric gas flow rate in the bed, cm. ³ /sec.
h	axial distance along bed, cm.
H	moving-bed height, cm.
h_f	heat transfer coefficient, cal./cm. ² K. sec.
Δh_n	length of the n -th compartment, cm.
$-\Delta H$	heat of reaction, cal./gm. carbon
k	reaction rate constant of carbon, atm. ⁻¹ hr. ⁻¹
L_f	fluid-bed height, cm.
N	total number of compartments
n	n -th compartment or one minus inerts mole fraction
p_{H_2}	hydrogen partial pressure, atm.
q_1, q_2	ratio of solid downflow rate and solid upflow rate to the solid feed rate, respectively
Q_T	heat generated in the moving bed, cal./sec. cm. ³
t	time, sec.
T	average bed temperature, K.
T_g	average gas temperature, K.
T_p	average particle temperature, K.
u_o	superficial gas velocity, cm./sec.
u_B	bubble rising velocity, cm./sec.
u_{mf}	superficial gas velocity at minimum fluidization, cm./sec.
V_{Bn}, V_{en}	volume of the bubble and emulsion phase at the n -th compartment, cm. ³
V_s	downward char rate in moving bed, cm./sec.
w_g, w_{go}, w_{gh}	total gas rate through the bed, moles/sec.
w_{Ho}	feed rate of hydrogen gas, moles/sec.

- W_{so} coal feed rate, gm./sec.
 \bar{W}_s average char rate in moving bed, gm./sec.
 X total fractional carbon conversion
 Y_{Bn}, Y_{en} nondimensional partial pressure of hydrogen in bubble and emulsion phase at n -th compartment, respectively
 Y_{Ho} hydrogen concentration in feed gas, mole/cm.³
 Y'_{co} initial carbon content in feed coal, $Y_{co} = Y'_{co}(1-X_0)$
 Y_M methane concentration, mole/cm.³
 Z carbon conversion based on the feed char, $Z \equiv (X-X_0)/(1-X_0)$
 Z_1, Z_{1F} outlet carbon conversion from moving bed and fluidized bed, respectively
 α_c number of moles of hydrogen reacted with one gram of carbon, mole/gm.
 ϵ_{mf} void fraction in emulsion phase
 n nondimensional time
 θ residence time in moving bed, sec.
 λ number of moles of hydrogen reacted with one mole of carbon, mole/mole
 ρ_b char bulk density, gm./cm.³
 ρ_p char particle density, gm./cm.³
 ρ_{co} density of feed coal, gm./cm.³
Subscript
 0 inlet
 1 outlet
 B bubble phase
 e emulsion phase
 n n -th compartment

BIBLIOGRAPHY

1. Kato, K. and C. Y. Wen. Chem. Engrg. Sci. 24, 1351 (1969).
2. Feldmann, H. F., J. A. Mima and P. M. Yavorsky. Coal Gasification. Advances in Chemistry Series, 131, A.C.S., Wash., D.C., p. 108 (1974).
3. Chermin, H. A. G. and D. W. Van Krevelen. Fuel, 36, 85 (1957).
4. Van Krevelen, D.W., C. Van Heerden and F. J. Huntjens. Fuel, 30, 253 (1951).
5. Pitt, G. J. Fuel, 41, 267 (1962).
6. Feldkirchner, H. L. and H. R. Linden. I. & E.C. Process Design and Development, 21, 153 (1963).
7. Wen, C. Y. and J. Huebler. I. & E.C. Process Design and Development, 4, 142 and 149 (1965).
8. Wen, C. Y., R. C. Bailie, C. Y. Lin, and W. S. O'Brien. Coal Gasification, Advances in Chemistry Series, 131, A.C.S., Wash., D.C., p. 9 (1974).
9. Feldmann, H. F., W. H. Simons, J. A. Mima and R. W. Hiteshue. A.C.S. Div. of Fuel Chem. Preprints, v. 14, No. 4, Part II, p. 1, Sept. 1970.
10. Feldmann, H. F. and P. M. Yavorsky. Paper presented at the 5th A.G.A./O.C.R. Synthetic Pipeline Gas Symposium, Chicago, Ill., Oct. 1973.
11. Feldmann, H. F., W. H. Simons, C. Y. Wen and P. M. Yavorsky. Paper presented at the 4th International Congress of Chem. Engrg., Chemical Equipment, Design and Automation, Marianske Laxne, Czechoslovakia, Sept. 1972.
12. Feldmann, H. F., C. Y. Wen, W. H. Simons and P. M. Yavorsky. Paper presented at the 71st National Meeting, A.I.Ch.E., Dallas, Tex., 1972.
13. Feldmann, H. F., K. D. Kiang and P. M. Yavorsky. A.C.S. Div. of Fuel Chem. Preprints, v. 15, No. 3, p. 62, Sept. 1971.
14. Wen, C. Y. and Y. H. Yu. A.I.Ch.E. J., 6, 220 (1960).
15. Yoshida, K. and C. Y. Wen. Chem. Engrg. Sci., 25, 1395 (1970).
16. Ishida, M. and C. Y. Wen. Chem. Engrg. Sci., 23, 125 (1968).
17. Mori, S. and C. Y. Wen. Paper presented at the 67th A.I.Ch.E. Annual Meeting,

Wash., D.C., Dec. (1974).

18. Mori, S. and C. Y. Wen. Paper submitted in I. & E.C. Process Design and Development (1974).
19. Hovmand, S. and J. F. Davidson. Fluidization, Chapt. 5, Academic Press (1971).
20. Miyauchi, T. Chem. Engrg., Tokyo, 26, 999 (1962).
21. Lewis, P. S., S. Friedman and R. W. Hiteshue. Fuel Gasification, Advances in Chemistry Series, 69, A.C.S., Wash., D.C., p. 50, (1967).
22. Johnson, J. L. Coal Gasification, Advances in Chemistry Series, 131, A.C.S., Wash., D.C., p. 145 (1974).

APPENDIX A

Solution of Equation (35)

The function $F(Z)$ in equation (35) has three different forms as defined by equations (2) and (34) depending upon the total fractional carbon conversion. When the total fractional carbon conversion, X , is less than 0.45, λ has the constant value 1.0 and $F(Z) = 0$. The integral for this case is then very simple. When X is between 0.45 and 0.55, λ has a value that varies linearly with X and $F(Z)$ turns out to be a parabolic function. For this case the integral of equation (35) is evaluated in two steps: first, for X up to 0.45 and $F(Z) = 0$; and second, for 0.45 up to the measured value of X and $F(Z)$ as a parabolic function. Thus k_1 and k_2 correspond to the values of the first and second parts of the integral. When X is larger than 0.55, λ has the constant value 1.8 and $F(Z)$ is a linear function of Z . For this case the same procedure as used previously results in three parts for the integral corresponding to k_1 , k_2 , and k_3 . These results are summarized by the following equations.

Case 1: $X < 0.45$

$$F(Z) \approx 0$$

$$k = \frac{1}{P_T \theta A} \ln \left[\frac{1 - \frac{BZ_H}{A+B}}{1 - Z_H} \right] \quad (A1)$$

Case 2: $0.45 \leq X \leq 0.55$

$$F(Z) \approx aZ^2 + bZ + c$$

$$\text{where } a = 4(1-X_o)$$

$$b = 8X_o - 3.6$$

$$c = 4(0.45 - X_o)^2 / (1 - X_o)$$

$$k = k_1 + k_2$$

$$k_2 = \frac{1}{P_T \theta} \left\{ -\frac{1}{2n} \ln \left[\frac{\bar{Z}_1}{\bar{Z}_2} \right] - \left(\frac{1 - BC'}{2C} \right) \ln \left[\frac{(1-Z_H)^2}{(1-Z_1)^2} \left(\frac{\bar{Z}_1}{\bar{Z}} \right) \right] + \left[\frac{\bar{b}}{2n} + Bb' + \frac{\bar{b}(1-BC')}{2C} \right] \frac{2}{\sqrt{q}} \right. \\ \left. \left[\tan^{-1} \left(\frac{2\bar{a}(1-Z_H) + \bar{b}}{\sqrt{q}} \right) - \tan^{-1} \left(\frac{2\bar{a}(1-Z_1) + \bar{b}}{\sqrt{q}} \right) \right] \right\} \quad (A2)$$

$$\text{where } \bar{a} = -4nB(1-X_o)$$

$$\bar{b} = B(1-nb')$$

$$\bar{C} = A - nBC'$$

$$q = 4\bar{a}\bar{C} - \bar{b}^2, q > 0$$

$$b' = -(2a + b)$$

$$C' = (a + b + C)$$

$$Z = \bar{a}(1-Z_H)^2 + \bar{b}(1-Z_H) + \bar{C}$$

$$\bar{Z}_1 = \bar{a}(1-Z_1)^2 + \bar{b}(1-Z_1) + \bar{c}$$

$$Z_1 = 1 - (0.45 - X_0)/(1-X_0)$$

Case 3: $X > 0.45$

$$F(Z) = 0.8Z + (0.8X_0 - 0.40)/(1-X_0)$$

$$k = k_1 + k_2 + k_3$$

$$k_3 = \frac{1}{P_T} \left\{ -\frac{D}{G} \ln \left[\frac{J + G(1-Z_H)}{J + G(1-Z_2)} \right] + \frac{E}{J} \ln \left[\frac{J + G(1-Z_H)}{J + G(1-Z_2)} \cdot \frac{1-Z_2}{1-Z_H} \right] \right\} \quad (A3)$$

where $D = 0.80B$

$$E = 0.8B - B(0.8X_0 - 0.40)/(1-X_0)$$

$$G = (1 + 0.8n)B$$

$$J = A + n(E-1)$$

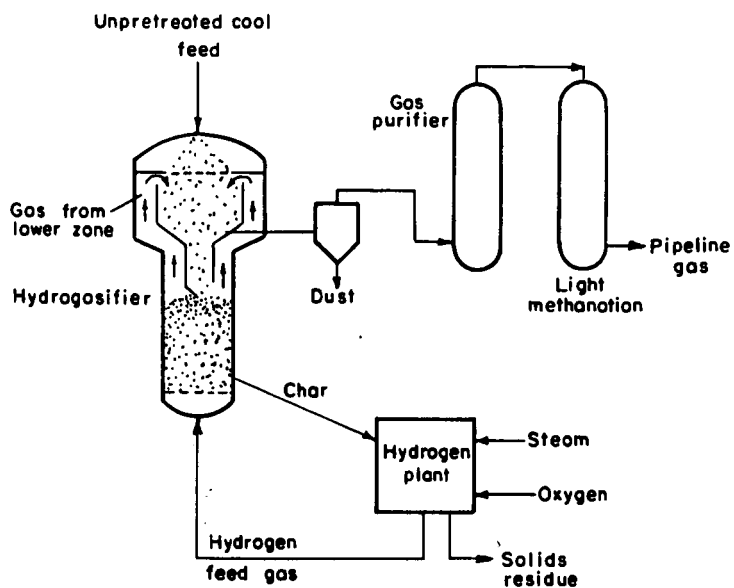


FIGURE I - The hydrane process for producing high BTU gas by the direct reaction of coal with hydrogen .

I-21-74

L-13603

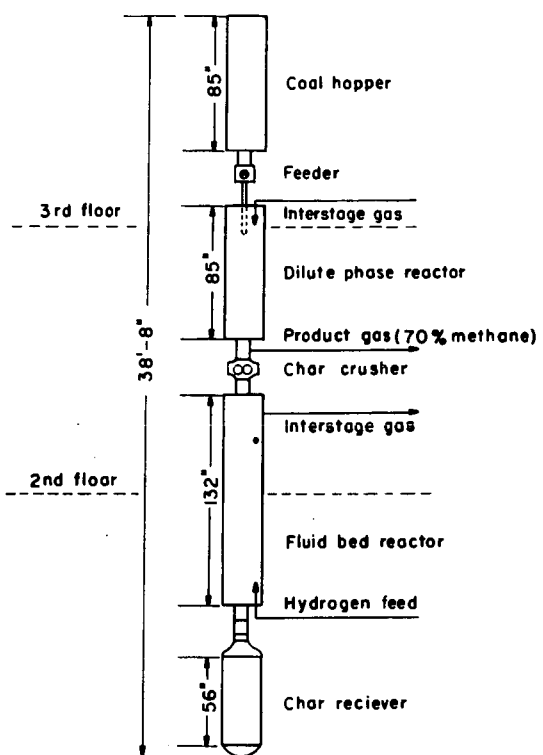


Figure 2 - Integrated hydrogasification unit.

L- I2914

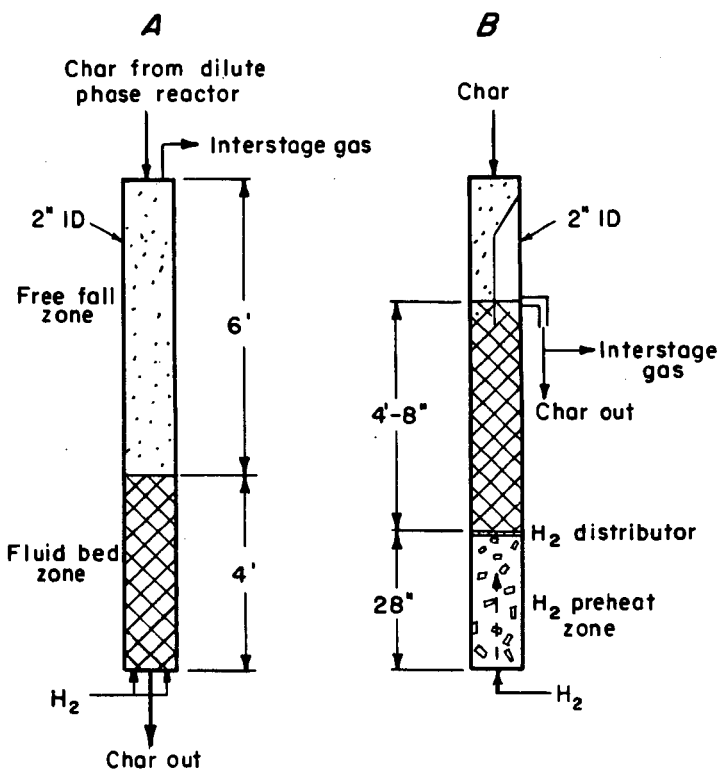


Figure 3—Schematics of fluid bed reactors

L-14051

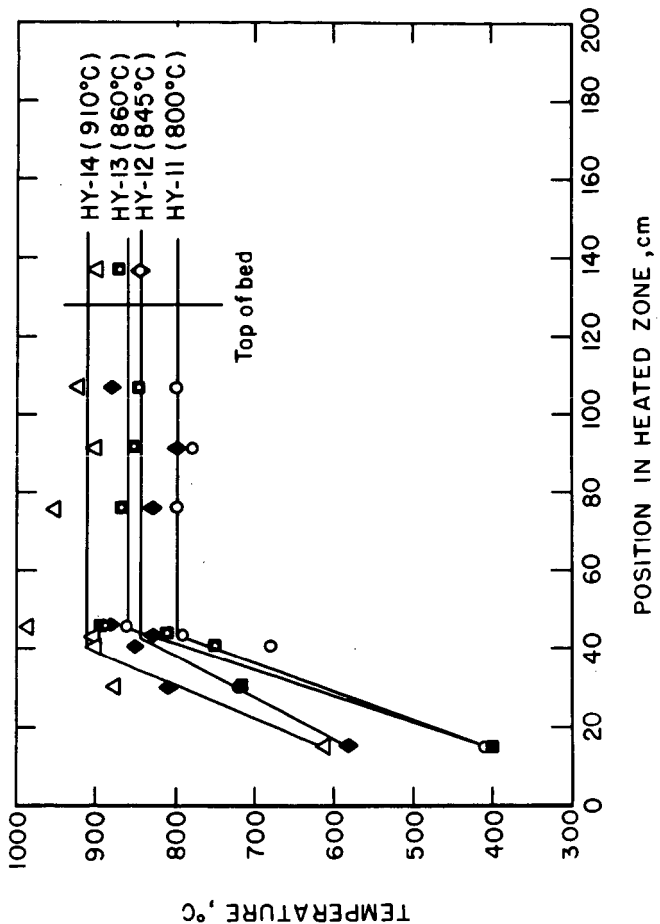


FIGURE 4- Temperature profiles for scheme A fluid bed reactor.
L-14050

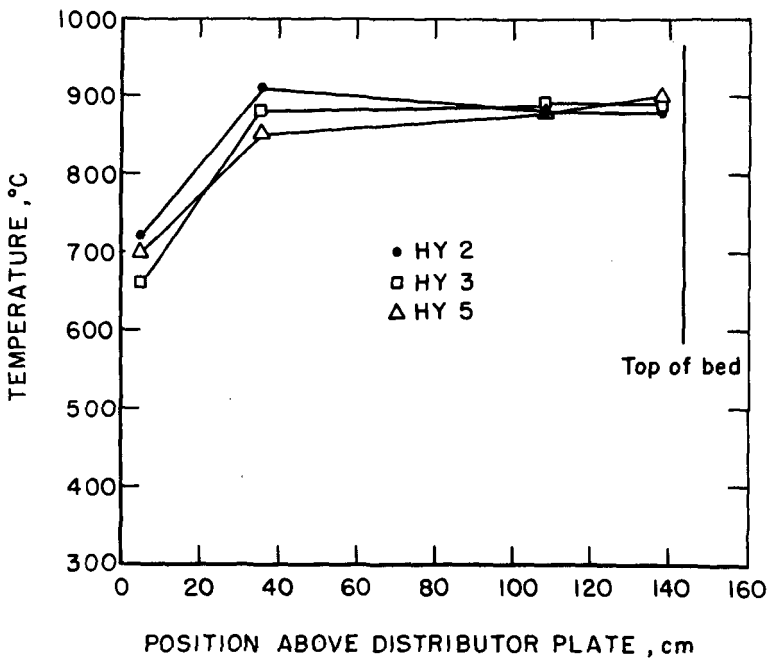


FIGURE 5 - Temperature profiles for scheme B fluid bed reactor.

L-14043

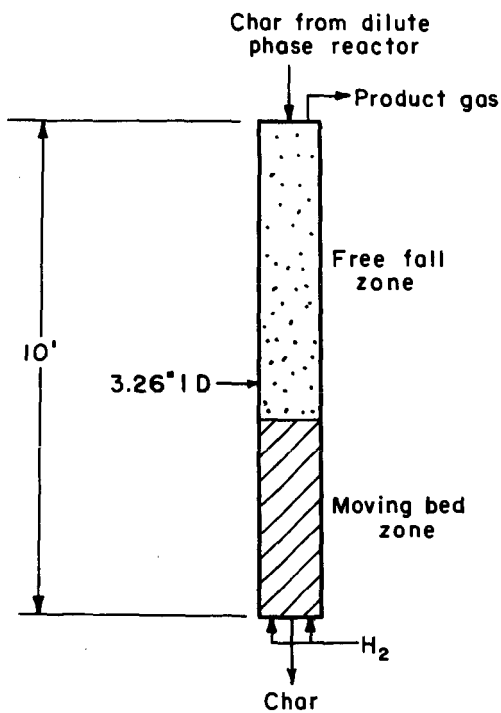


Figure 6—Schematic of moving bed reactor

L-14056

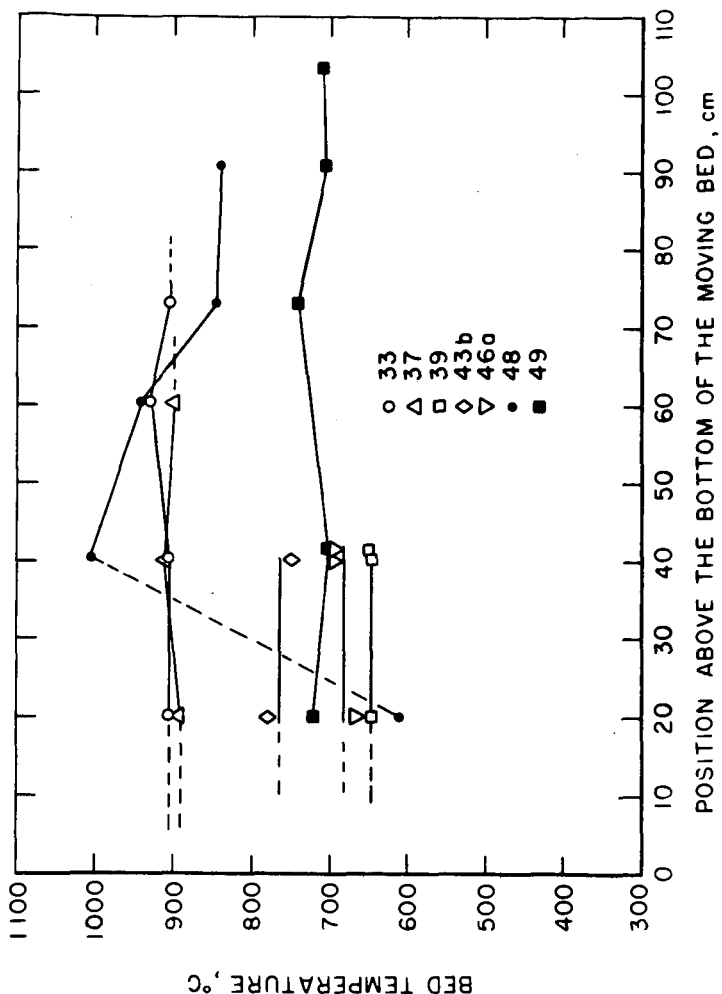


FIGURE 7 - Temperature profiles for the moving bed reactor

L-14044

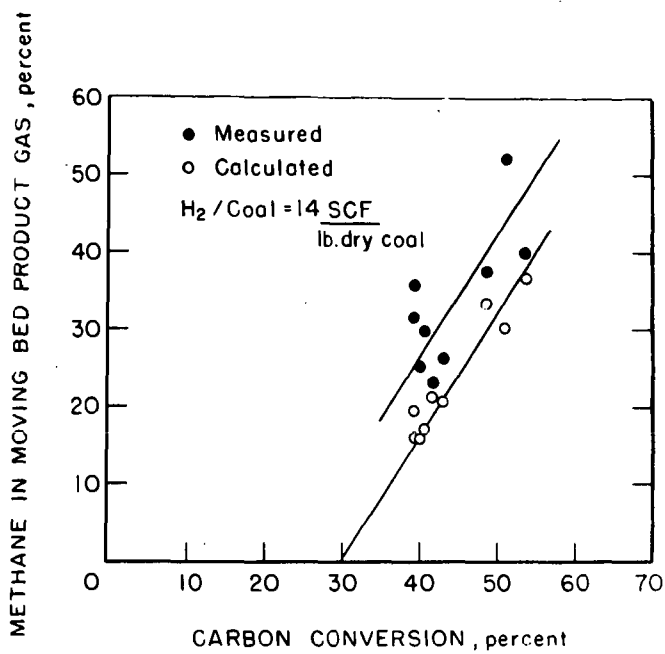


FIGURE 8 - Mixing effect on the moving bed product gas near the sampling point.

L-14042

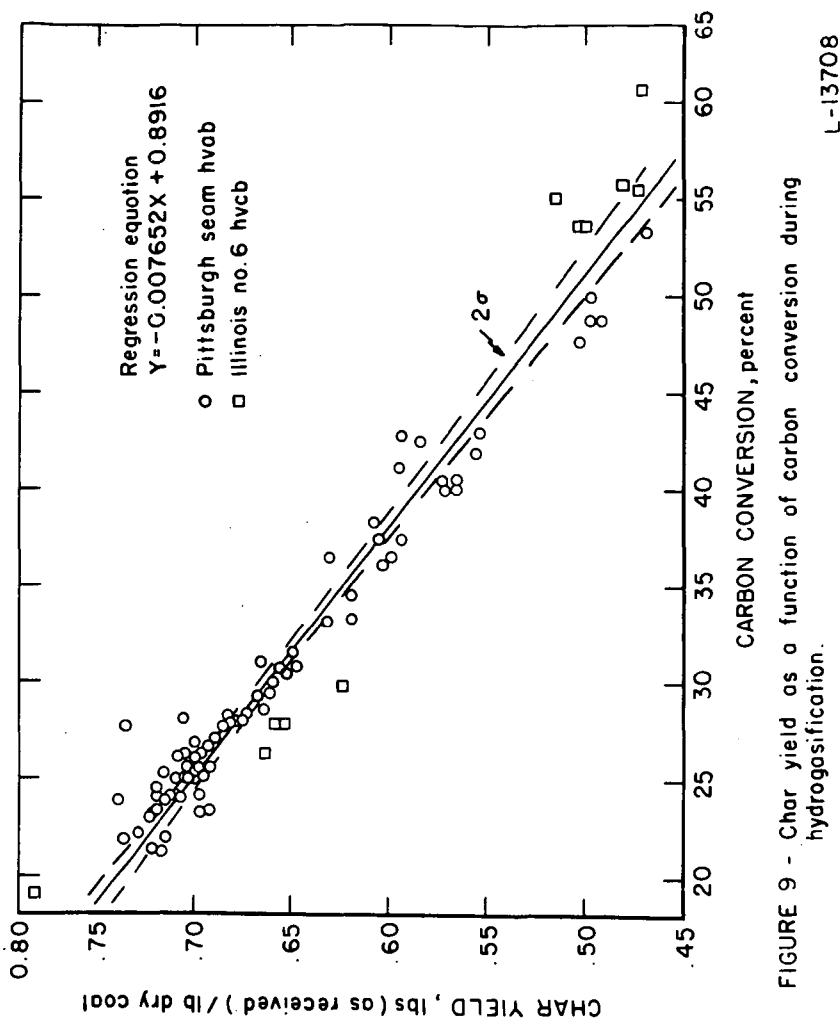


FIGURE 9 - Char yield as a function of carbon conversion during hydrogasification.

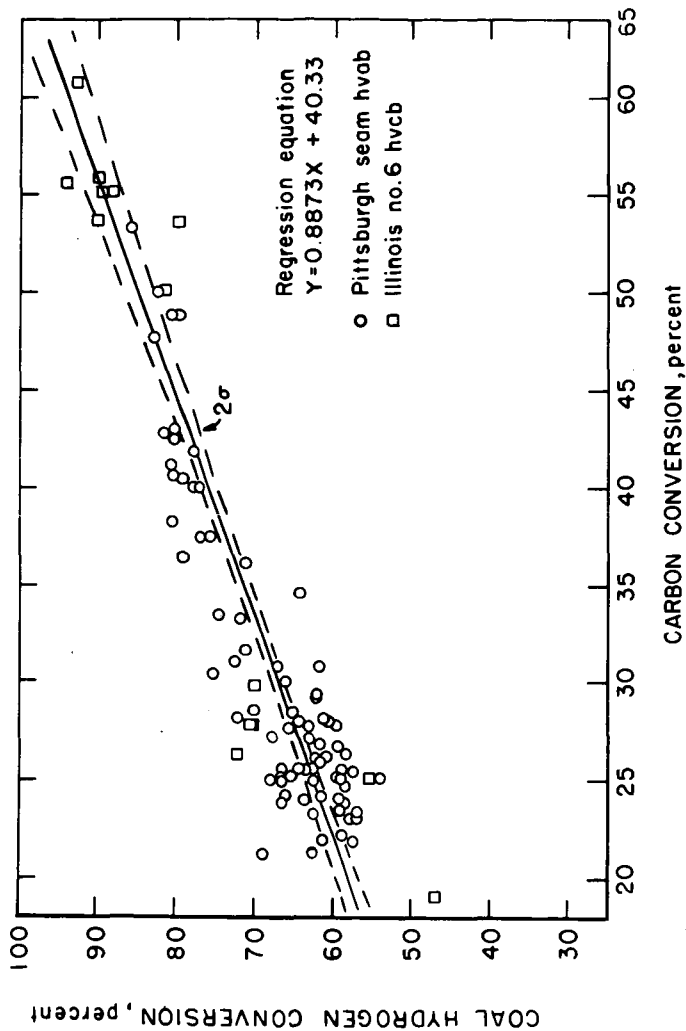


FIGURE 10 - Coal hydrogen conversion as a function of carbon conversion during hydrogasification.

L-13709

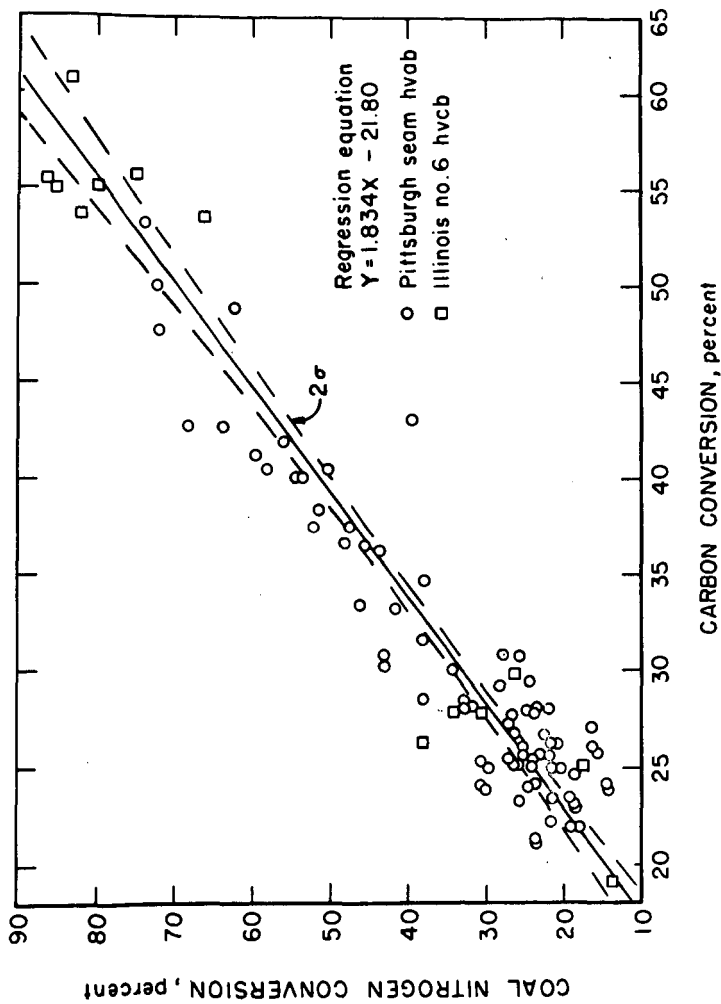


FIGURE II - Coal nitrogen conversion as a function of carbon conversion during hydrogasification.

L-13712

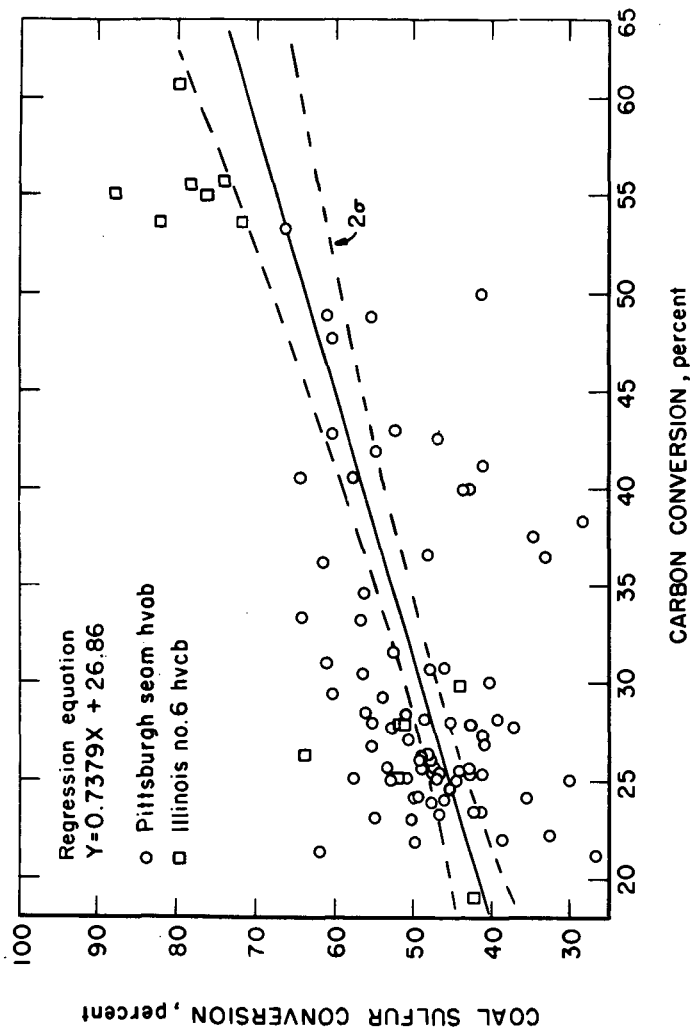


FIGURE 12 - Sulfur conversion as a function of carbon conversion during hydrogasification.

L-13710

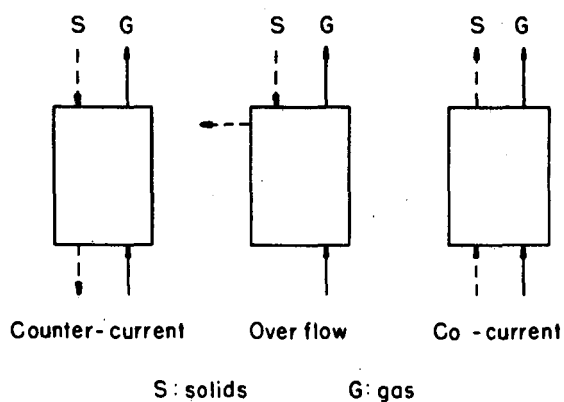


FIGURE I3 - Modes of the fluidized bed operations.

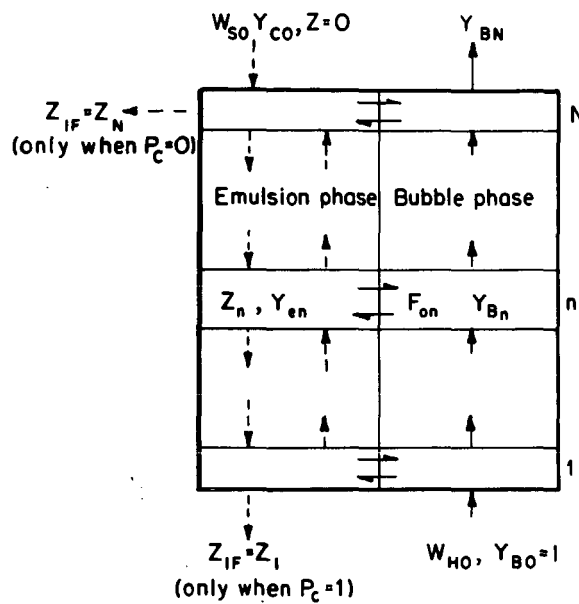


Figure 14 - Bubble assemblage model for
fluidized char gasification

L-14046

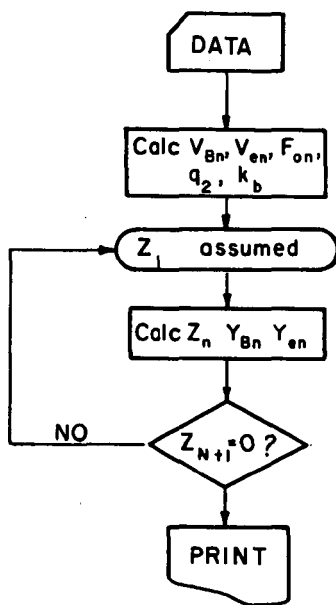


Figure 15 - Computer logic diagram

L-14049

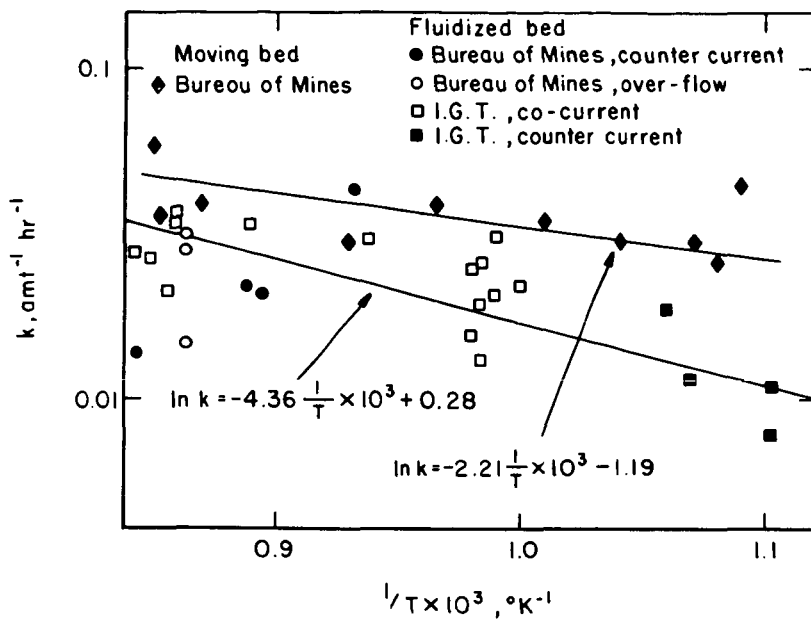


FIGURE 16 - Effect of average bed temperatures on rate constants for char hydrogasification

L-14047

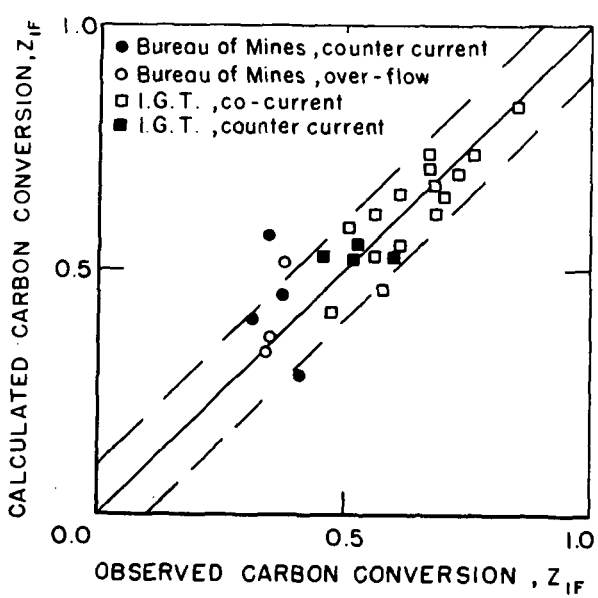


FIGURE 17- Comparison of calculated and observed carbon conversions in fluidized char hydrogasification experiments.

L-14048

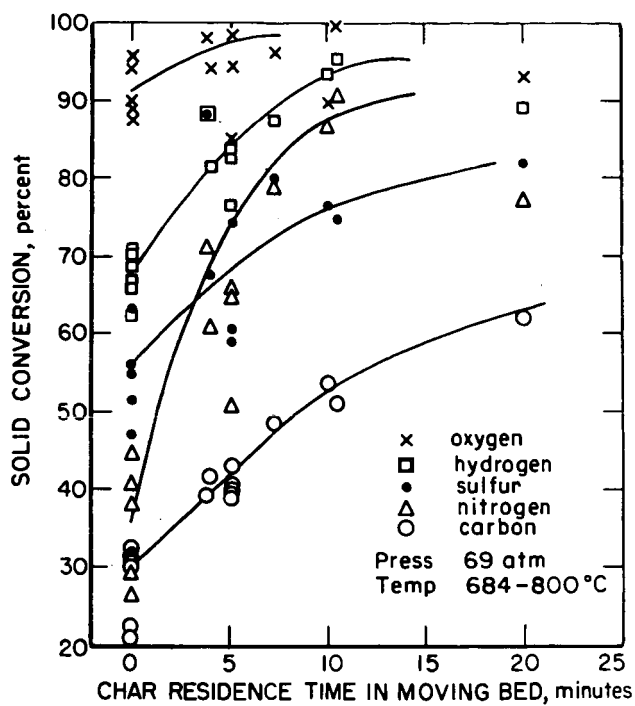


Figure 18 - Cool constituent conversion as function of residence time

L-13954